

論文 / 著書情報
Article / Book Information

Title	Estimation of electron temperature and density of the decay plasma in a laser-assisted discharge plasma extreme ultraviolet source by using a modified Stark broadening method
Authors	Qiushi Zhu, Takahiro Muto, Junzaburo Yamada, Nozomu Kishi, Masato Watanabe, Akitoshi Okino, Kazuhiko Horioka, Eiki Hotta
Citation	J. Appl. Phys., Vol. 110, ,
発行日/Pub. date	2011, 12
公式ホームページ /Journal home page	http://jap.aip.org/
権利情報/Copyright	Copyright (c) 2011 American Institute of Physics

Estimation of electron temperature and density of the decay plasma in a laser-assisted discharge plasma extreme ultraviolet source by using a modified Stark broadening method

Qiushi Zhu, Takahiro Muto, Junzaburo Yamada, Nozomu Kishi, Masato Watanabe et al.

Citation: *J. Appl. Phys.* **110**, 123302 (2011); doi: 10.1063/1.3672816

View online: <http://dx.doi.org/10.1063/1.3672816>

View Table of Contents: <http://jap.aip.org/resource/1/JAPIAU/v110/i12>

Published by the [American Institute of Physics](#).

Related Articles

Terahertz generation from laser filaments in the presence of a static electric field in a plasma
[Phys. Plasmas](#) **18**, 123106 (2011)

Comparison of the electron density measurements using Thomson scattering and emission spectroscopy for laser induced breakdown in one atmosphere of helium
[Appl. Phys. Lett.](#) **99**, 261504 (2011)

Intense terahertz emission from atomic cluster plasma produced by intense femtosecond laser pulses
[Appl. Phys. Lett.](#) **99**, 261503 (2011)

Plasma-based multistage virtual cathode radiation
[Phys. Plasmas](#) **18**, 123104 (2011)

Gd plasma source modeling at 6.7nm for future lithography
[Appl. Phys. Lett.](#) **99**, 231502 (2011)

Additional information on J. Appl. Phys.

Journal Homepage: <http://jap.aip.org/>

Journal Information: http://jap.aip.org/about/about_the_journal

Top downloads: http://jap.aip.org/features/most_downloaded

Information for Authors: <http://jap.aip.org/authors>

ADVERTISEMENT

**AIP**Advances

Submit Now

**Explore AIP's new
open-access journal**

- **Article-level metrics
now available**
- **Join the conversation!
Rate & comment on articles**

Estimation of electron temperature and density of the decay plasma in a laser-assisted discharge plasma extreme ultraviolet source by using a modified Stark broadening method

Qiushi Zhu,^{a)} Takahiro Muto, Junzaburo Yamada, Nozomu Kishi, Masato Watanabe, Akitoshi Okino, Kazuhiko Horioka, and Eiki Hotta

Department of Energy Sciences, Tokyo Institute of Technology, Yokohama, Japan

(Received 15 September 2011; accepted 1 December 2011; published online 30 December 2011)

In order to investigate the plasma expansion behaviors and the electrical recovery process after the maximum implosion in our tin fueled laser-assisted discharge plasma (LDP) 13.5 nm EUV source, we developed and evaluated a cost-efficient spectroscopic method to determine the electron temperature T_e and density n_e simultaneously, by using Stark broadenings of two Sn II isolated lines ($5s^24f^2F^{\circ}_{5/2}-5s^25d^2D_{3/2}$ 558.9 nm and $5s^26d^2D_{5/2}-5s^26p^2P^{\circ}_{3/2}$ 556.2 nm) spontaneously emitted from the plasma. The spatial-resolved evolutions of T_e and n_e of the expansion plasma over 50 to 900 ns after the maximum implosion were obtained using this modified Stark broadening method. According to the different n_e decay characteristics along the Z-pinch axis, the expansion velocity of the electrons was estimated as $\sim 1.2 \times 10^4$ ms⁻¹ from the plasma shell between the electrodes towards the cathode and the anode. The decay time constant of n_e was measured as 183 ± 24 ns. Based on the theories of plasma adiabatic expansion and electron-impact ionization, the minimum time-span that electrical recovery between the electrodes needs in order to guarantee the next succeeding regular EUV-emitting discharge was estimated to be 70.5 μ s. Therefore, the maximum repetition rate of our LDP EUV source is ~ 14 kHz, which enables the output to reach 125 W/(2 π sr). © 2011 American Institute of Physics. [doi:10.1063/1.3672816]

I. INTRODUCTION

Extreme ultraviolet (EUV) lithography is considered the most promising candidate for semiconductor manufacturing of the half-pitch 22 nm node and beyond.¹ The light source for EUV lithography (EUVL), 13.5 nm in-band (2% bandwidth) EUV emission, is obtained from hot and dense plasmas created mainly by pulsed laser ablation [laser produced plasma (LPP)] or discharge current constriction [discharge produced plasma (DPP)].² In order to apply EUVL to high volume manufacturing, the power of the EUV source is still the most critical issue,³ and increasing the repetition rate is one of the most effective ways to scale up the source power.

Tin fueled laser-assisted discharge plasma (LDP) proves to be a powerful light source for the generation of sufficient in-band 13.5 nm EUV emission.⁴⁻⁷ LDP is also of great commercial interest because of its preferable conversion efficiency^{8,9} and simplicity compared to other methods. In the LDP source, 13.5 nm EUV emission is generated from the hot and dense Z-pinch implosion plasma created by a laser triggered vacuum arc.¹⁰ After the maximum implosion, plasmas between the electrodes expand into the vacuum. The plasma expansion process directly determines the time span that the electrical recovery requires before the next regular discharge can take place. Here, with the intention of estimating the minimum discharge interval, or the maximum repetition rate, of our LDP source, we report investigation results

on the behaviors and parameters of the expansion plasma between the electrodes after a single discharge.

Using the Stark broadening of an isolated spectral line to determine the electron density n_e at a known electron temperature T_e is very simple and inexpensive compared to interferometry, Thomson scattering, and other spectroscopic methods.¹¹ However, there is currently no simple and non-intrusive method for obtaining the T_e of non-local thermal equilibrium (LTE) high-atomic-number plasmas.¹² In this work, we develop and evaluate a modified Stark broadening method that can determine n_e and T_e simultaneously using the Stark widths of two Sn II isolated lines spontaneously emitted from the plasma. This method is referred to as the cross-point or intersection method.

This cross-point or intersection method, using the Stark broadening of hydrogen lines, was adopted by other research groups to simultaneously determine the n_e and T_e of plasmas, and the results proved to be in good agreement with those obtained from other measurements.¹³ In our study, a similar intersection Stark broadening method is developed using the spectral lines of Sn II instead of hydrogen to obtain parameters of the expansion plasma after a discharge in the LDP source. Considering that the theoretical calculation of the Stark widths of high atomic number (Z) atomic and ionic lines cannot be as accurate as the calculated hydrogen and helium lines,¹² the validity of the intersection Stark broadening method using Sn II lines is discussed in relation to a “verification experiment.” In this experiment, a tin fueled low current (several kilo-amperes) arc discharge is triggered in a pure helium atmosphere. Line profiles of the Sn II and He I spectra emitted from the discharge produced plasma in

^{a)}Author to whom correspondence should be addressed. Electronic mail: zhu.q.ab@m.titech.ac.jp.

the same condition are recorded. Based on the measured Sn II Stark widths and the proposed intersection Stark broadening method, the T_e and n_e of the plasma are estimated, and the results are used to calculate the line profiles of a He I line. The correlation between these calculated profiles and the measured He I spectra is used to verify the validity of the intersection Stark broadening method.

In Sec. II, the theoretical approach of the intersection Stark broadening method using Sn II lines to determine n_e and T_e is presented, and a thorough calculation of a He I line profile for method verification is conducted. In Sec. III, the experimental setup of our LDP source and the diagnostic equipment is introduced. In Secs. IV and V, results of the verification experiment and the electron density and temperature of the expansion plasma in the LDP source are presented. The diffusion process of the discharge produced EUV-emitting plasma and the maximum discharge repetition rate are discussed. Finally, conclusions are summarized in Sec. VI.

II. STARK BROADENING

A. Intersection method using Sn II lines

The Stark broadening of a spectral line (Lorentz profile) depends on the local field of both electrons and ions in a plasma. However, for lines emitted from multi-electron systems, ions are much less important as perturbing particles than are electrons.¹¹ Therefore, in the calculation of Stark widths of Sn atomic or ionic lines, only electron impact broadening is considered. The Stark width is calculated from the following widely used semiempirical equations:¹⁴

$$\begin{aligned} \omega_{if} = & 8 \left(\frac{\pi}{3} \right)^{3/2} \frac{\hbar}{m_e a_0} n_e \left(\frac{E_H}{k_B T_e} \right)^{1/2} \\ & \times \sum_{i', f'} \left[\left| \langle i' | \vec{r} | i \rangle \right|^2 \bar{g}_{se} \left(\frac{\bar{E}}{|\Delta E_{i',i}|} \right) \right. \\ & \left. + \left| \langle f' | \vec{r} | f \rangle \right|^2 \bar{g}_{se} \left(\frac{\bar{E}}{|\Delta E_{f',f}|} \right) \right], \quad (1) \end{aligned}$$

where ω_{if} is the half-width at half-maximum of the Stark width of the spectral line from energy level i (initial) to f (final). The subscripts i' and f' refer to the perturbing energy levels of levels i and f . \bar{E} is the energy of the colliding electrons, E_H is the hydrogen ionization energy, a_0 is the Bohr radius, \vec{r} is the bound electron position operator, and \bar{g}_{se} is the Gaunt factor.^{15,16} The other variables retain their original meanings. The atomic matrix elements are calculated from

$$\left| \langle i' | \vec{r} | i \rangle \right|^2 = \frac{3E_H}{\Delta E_{i',i}} a_0^2 f_{i',i},$$

where $f_{i',i}$ is the oscillation strength of the transition from i' to i ,¹¹ with the assumption that the electron velocity follows the Maxwellian distribution $\bar{E} = \frac{3}{2} k_B T_e$. Therefore, the Stark width depends not only on n_e , but also on T_e .

In our study, we chose Sn II $5s^2 4f^2 F^\circ_{5/2} - 5s^2 5d^2 D_{3/2}$ (558.9 nm) and $5s^2 6d^2 D_{5/2} - 5s^2 6p^2 P^\circ_{3/2}$ (556.2 nm) lines, based on the following three reasons:

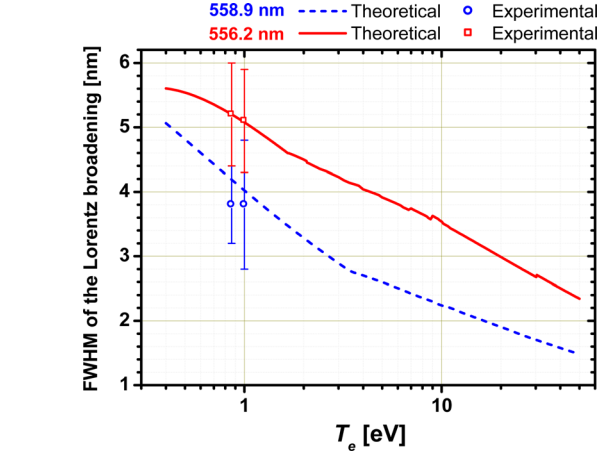


FIG. 1. (Color online) Calculation results of the Stark broadening FWHM of Sn II $5s^2 4f^2 F^\circ_{5/2} - 5s^2 5d^2 D_{3/2}$ (558.9 nm, dash line) and $5s^2 6d^2 D_{5/2} - 5s^2 6p^2 P^\circ_{3/2}$ (556.2 nm, solid line) lines vs electron temperature T_e at electron density $n_e = 1.0 \times 10^{18} \text{ cm}^{-3}$. The corresponding experimental Stark broadening (blue open circles and red open squares) is taken from Refs. 23 and 24.

- (1) A larger amount of Sn II ions than Sn I atoms exists in the diffusion plasma after the discharge.
- (2) More complete and accurate information about the energy states and oscillation strength of Sn II than of the higher charge state of Sn ions is obtainable.
- (3) The two lines can be recorded together in a single measurement.

The atomic information needed in order to calculate the electron impact Stark widths of these two Sn II lines comes from Refs. 17–22 or is calculated according to Eq. (36) in Ref. 14.

The calculation results of the Stark full width at half-maximum (FWHM) versus T_e of Sn II $5s^2 4f^2 F^\circ_{5/2} - 5s^2 5d^2 D_{3/2}$ (558.9 nm) and $5s^2 6d^2 D_{5/2} - 5s^2 6p^2 P^\circ_{3/2}$ (556.2 nm) lines at $n_e = 1.0 \times 10^{18} \text{ cm}^{-3}$ is shown in Fig. 1. A comparison between our calculations and the experimental results published in Refs. 23, 24 displays good agreement. The Stark-width-ratio of these two lines versus T_e , which is independent of n_e , as indicated in Eq. (1), is shown in Fig. 2. This curve can be used to determine T_e with the measured Stark-width-ratio. With the known T_e and measured Stark width of either spectral line, n_e can be obtained using Fig. 1, because the Stark width is proportional to n_e , as shown in Eq. (1). Note that the T_e application range of this intersection Stark broadening method depends on the spectral lines we choose. The curve in Fig. 2 indicates that the T_e estimation using the above-mentioned two Sn II lines is applicable for relatively low temperature plasma with $T_e \leq 10 \text{ eV}$.

B. He I line profile

Accurate calculation of a He I spectral line is needed in order to verify the validity of our intersection Stark broadening method. A thorough calculation of Stark profiles of He atomic lines includes both electron and ion impact broadenings, as discussed in Refs. 25 and 11. For the electron impact broadening, the Lorentz width calculation (Eq. (3.15) in Ref. 25) consists of a strong collision term (in the high

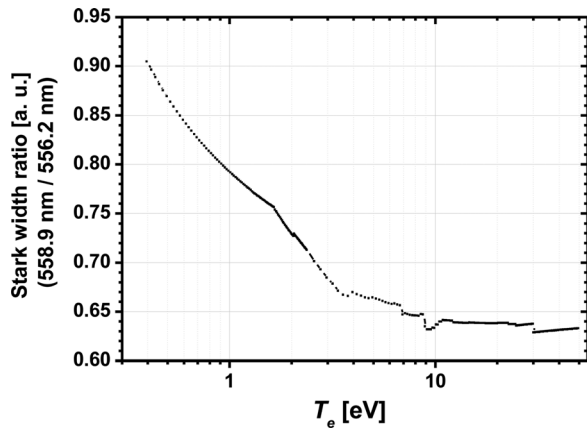


FIG. 2. Calculated results of the Stark-width-ratio of Sn II $5s^24f^2F^{\circ}_{5/2}-5s^25d^2D_{3/2}$ (558.9 nm) and $5s^26d^2D_{5/2}-5s^26p^2P^{\circ}_{3/2}$ (556.2 nm) lines vs electron temperature T_e .

temperature range) and a weak collision term (in the low temperature range). For the ion impact broadening, as a very small correction term to the total line broadening, the calculation assumes that the ion impact satisfies a quasi-static approximation, and the field strength follows a Holtsmark distribution with an ion charge state of $Z_i = 1$. The total Stark profile of an isolated He I line is obtained through the convolution of the electron impact profile with the ion broadening (Eq. (4.14) in Ref. 25).

In this article, the He I $1s3d^1D_2-1s2p^1P^{\circ}_1$ (667.8 nm) line profiles are calculated with the information about energy levels and oscillator strengths listed in Ref. 26. A calculation result of the Stark profile at $n_e = 1.06 \times 10^{23} \text{ cm}^{-3}$ and $T_e = 31\,000 \text{ K}$ is compared with the experimental and calculation results published by other researchers,²⁷ as shown in Fig. 3. Good agreement between our results and other profiles justifies the use of this He atomic transition as a calibration line. To obtain the

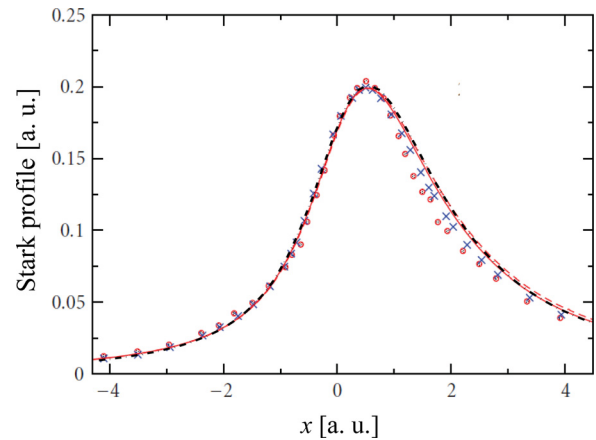


FIG. 3. (Color online) Calculated profile (black dashed line) for He I $1s3d^1D_2-1s2p^1P^{\circ}_1$ (667.8 nm) line at reduced wavelength (Ref. 27) at electron temperature $T_e = 31\,000 \text{ K}$ and electron density $n_e = 10.6 \times 10^{22} \text{ cm}^{-3}$. Comparison is made with other theoretical and experimental data listed in Ref. 27.

final emission line profile, Doppler broadening and instrumental broadening (both are Gaussian profile) are to be convoluted with the Stark profile. However, for the non-LTE plasma generated in our experimental conditions, the Doppler width is more than two orders less than the Stark width. Therefore, here we neglect the Doppler broadening and consider only Stark and instrumental broadenings.

III. EXPERIMENTAL SETUP

The schematic diagram of our LDP setup with the diagnostic systems is shown in Fig. 4 (left). This setup is also used for the above-mentioned verification experiment. A detailed description of this setup for EUV generation can be found in our previous article.¹⁰ Here, we only briefly

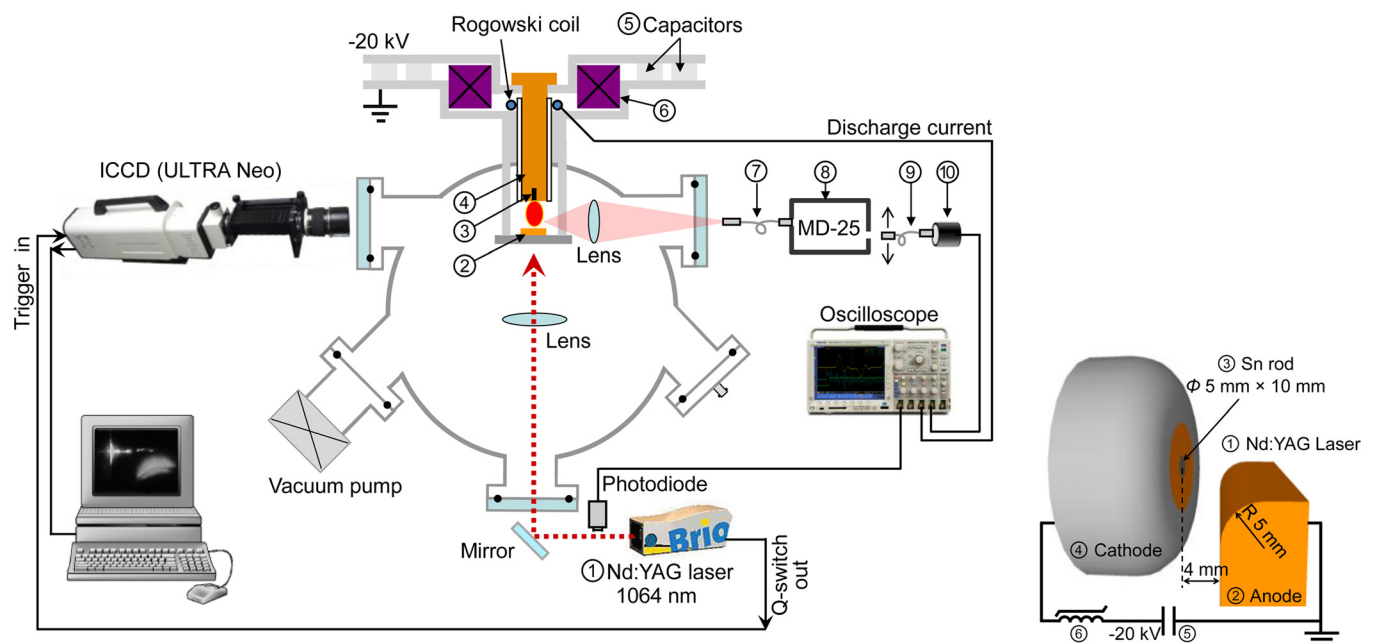


FIG. 4. (Color online) (Left) Experimental setup of our LDP source with the optical diagnostics systems, for both EUV generation and the method-verification-experiment. (1) Q-switched Nd:YAG laser, (2) anode, (3) tin rod, (4) cathode, (5) capacitors (80 nF) charging to a dc voltage, (6) magnetic core, (7) optical fiber, (8) spectrometer, (9) optical fiber, (10) PMT. (Right) Electrode arrangement of our LDP EUV source.

introduce the electrode arrangement of this setup, shown in Fig. 4 (right). The cathode consists of a tin rod with a diameter of 5 mm and its copper holder. The copper anode with a cross section, as shown in Fig. 4 [(2)], is grounded. The gap distance between the electrodes is 4 mm. A bank of ceramic capacitors with a total capacitance of 80 nF connecting the electrodes is charged to a dc potential. The initiating laser pulse from a Q-switched Nd:YAG laser operating in the single pulse mode with a 1064 nm wavelength, a 5 ns pulse width, and a 24 to 104 mJ tunable energy output is focused on the tin surface along the cathode axis by a convex lens with a focal length of 17 cm. The corresponding laser power density is on the order of 10^{11} W cm⁻². The setup operates in the single-shot-mode.

In the verification experiment for the intersection Stark broadening method, the dc voltage between the electrodes is -3.9 kV, and the discharge is triggered in pure helium gas at atmospheric pressure. The plasma emission at certain positions along the pinch axis is focused by a convex lens and conducted into the spectrometer (JASCO, MD-25) through an optical fiber. The grating inside the spectrometer is with 1800 lines/mm. The emission at a certain wavelength that exits from the spectrometer is intensified and recorded by a photo-multiplier tube (PMT) (Hamamatsu R2257) and an oscilloscope through another optical fiber (Ocean Optics, P400-2-AL/SR, entrance diameter 0.4 mm) with one end connected to the PMT and the other end facing the exit of the spectrometer and fixed onto an XY-stage. The optical emission spectrum is obtained by moving the XY-stage along the spectrum in the focal plane, as shown in Fig. 4 (left), with a 10 μ m spatial resolution. The spectral resolutions of this system are measured as 0.385 nm at 557 nm (Sn II lines) and 0.354 nm at 668 nm (He I line).

For 13.5 nm EUV generation, the chamber of this LDP source is evacuated to 10^{-5} Torr, and the dc voltage between the electrodes is -20 kV. The in-band EUV energy was estimated as 8.9 mJ/($2\pi sr$)/pulse, with an energy conversion efficiency of 1.65%. To investigate the expansion process of the EUV-emitting plasma in the decay phase, a visible-region intensified charge coupled device (ICCD) (ULTRA Neo) with a 100 ns exposure time and a 10 MHz frame rate is utilized to observe the plasma behavior after the maximum implosion. The EUV emission is recorded simultaneously by a 13.5 nm in-band calorimeter. To obtain the Sn II spectra emitted from the plasma, a similar spectroscopy system is adopted, but instead of the optical fiber and PMT ((9) and (10) in Fig. 4) a streak camera (DRS Imacon 468) is used with a spectral resolution of 0.020 nm.

IV. EXPERIMENTAL RESULTS

A. Verification experiment

In this experiment, discharges between the tin cathode and anode are triggered and conducted in pure He gas under atmospheric pressure. The discharge current with a peak value of 3 kA is shown as the red line in Fig. 5; the blue and black lines refer to the emission signals at 558.9 nm (Sn II, $5s^24f^2F^{\circ}_{5/2}-5s^25d^2D_{3/2}$) and 667.8 nm (He I, $1s3d^1D_2-1s2p^1P^{\circ}_1$) from the plasma at 2 mm from the tin surface in

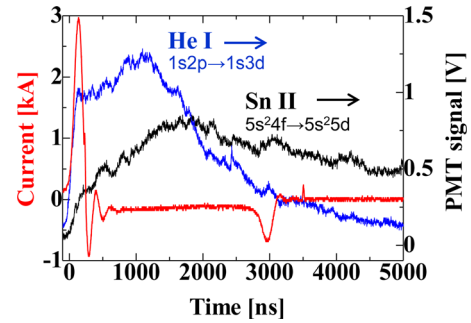


FIG. 5. (Color online) The discharge current, and the plasma emission signal at 558.9 nm (Sn II, $5s^24f^2F^{\circ}_{5/2}-5s^25d^2D_{3/2}$) and 667.8 nm (He I, $1s3d^1D_2-1s2p^1P^{\circ}_1$), as indicated in the figure, respectively. The discharge is conducted in pure He gas under atmospheric pressure; 0 ns refers to the current onset time.

the pinch axis. A value of 0 ns corresponds to the current onset time. Evolutions of the spectra are obtained by averaging signals from at least 5 discharges for each wavelength in every 50 ns. By deconvoluting the Lorentz broadening from the spectral line profiles with known instrumental broadening (Gauss profile) of 0.544 nm, the evolutions of the Stark widths and the width-ratios of Sn II $5s^24f^2F^{\circ}_{5/2}-5s^25d^2D_{3/2}$ (558.9 nm) and $5s^26d^2D_{5/2}-5s^26p^2P^{\circ}_{3/2}$ (556.2 nm) lines are obtained, as demonstrated in Fig. 6(a). Then, evolutions of electron density n_e and temperature T_e are deduced using the intersection Stark broadening method according to the calculated results in Figs. 2 and 1; the results are shown in Fig. 6(b). During the delay of 1050 ns to 1950 ns, n_e and T_e decay from 2.2×10^{17} cm⁻³ and 3.1 eV to 1.1×10^{17} cm⁻³ and 0.40 eV. Using these n_e and T_e data, the corresponding profiles of the He I $1s3d^1D_2-1s2p^1P^{\circ}_1$ (667.8 nm) line are calculated with the Stark width, shown as the black dashed line with squares in Fig. 6(c). The experimental Stark widths shown in the same figure are deconvoluted from the measured He I $1s3d^1D_2-1s2p^1P^{\circ}_1$ (667.8 nm) line profiles under identical experimental conditions. The deviation of the calculated results with respect to the experimental Stark width is illustrated in Fig. 7(d). Good agreement with the deviation within 10% is achieved when the electron temperature is larger than 1 eV (delay less than 1700 ns). Although when $T_e < 1$ eV the deviation increases up to 14.8%, it is still acceptable with regard to the calculation error. In general, the comparison result between the calculated and experimental He I line profiles confirms the validity of the intersection Stark broadening method using Sn II lines for the simultaneous estimation of n_e and T_e in discharge produced plasmas.

B. Characteristics of the plasmas in the decay phase

In this experiment, the discharge is triggered and conducted in vacuum with a pressure of 10^{-5} Torr. The 13.5 nm in-band EUV emits from the implosion plasma near the peak discharge current. The EUV emission characteristics and the corresponding plasma dynamics were elaborately discussed in our previous article.¹⁰ Here we focus on the plasma expansion process in the decay phase after the maximum implosion. Figures 7(a)-7(e) demonstrate the visualization of the plasma behaviors captured by an ICCD camera with a 100 ns

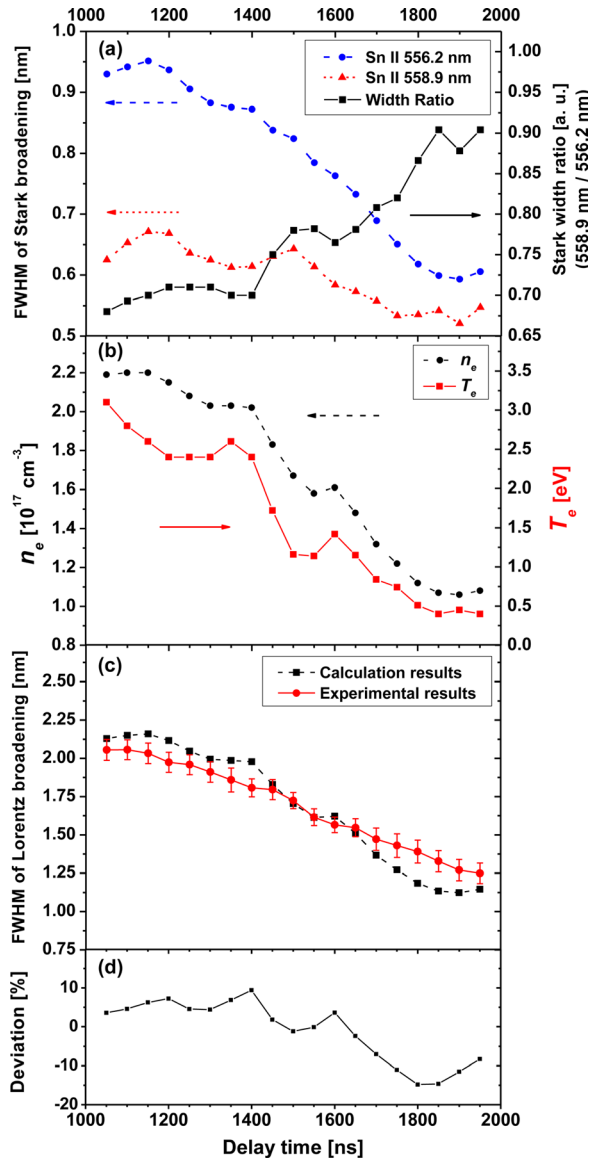


FIG. 6. (Color online) (a) Experimental evolution of the Stark-width-ratio of Sn II $5s^24f^2F^{\circ}_{5/2}-5s^25d^2D_{3/2}$ (558.9 nm) and $5s^26d^2D_{5/2}-5s^26p^2P^{\circ}_{3/2}$ (556.2 nm) lines. (b) Evolutions of electron density n_e and temperature T_e obtained via the intersection Stark broadening method. (c) Comparison between the experimental Stark broadening of He I $1s3d^1D_2-1s2p^1P^{\circ}_1$ (667.8 nm) line and the calculated results based on the electron density n_e and temperature T_e shown in (b). Red solid circles = experimental Stark widths; black squares = calculated results. (d) The deviation of the calculated results with respect to the experimental Stark width shown in (c). The discharge is triggered and conducted in pure He gas under atmospheric pressure.

gate time. The corresponding discharge current and EUV emission signal are shown in Fig. 7(f), with five broken lines indicating the start time of each plasma image. In Fig. 7(a), besides the needle-like implosion plasma, a large amount of plasma is seen attaching to the electrode surface. With the termination of the implosion, the pinched plasma expands much faster than the plasmas near the electrodes, as revealed in Fig. 7(b), where the implosion plasma completely disappears after 100 ns, whereas distinct plasmas still remain near the electrode surface. Meanwhile, a plasma layer with a shell-like shape between the electrodes appears due to the interaction of the quick expansion of the constricted plasma

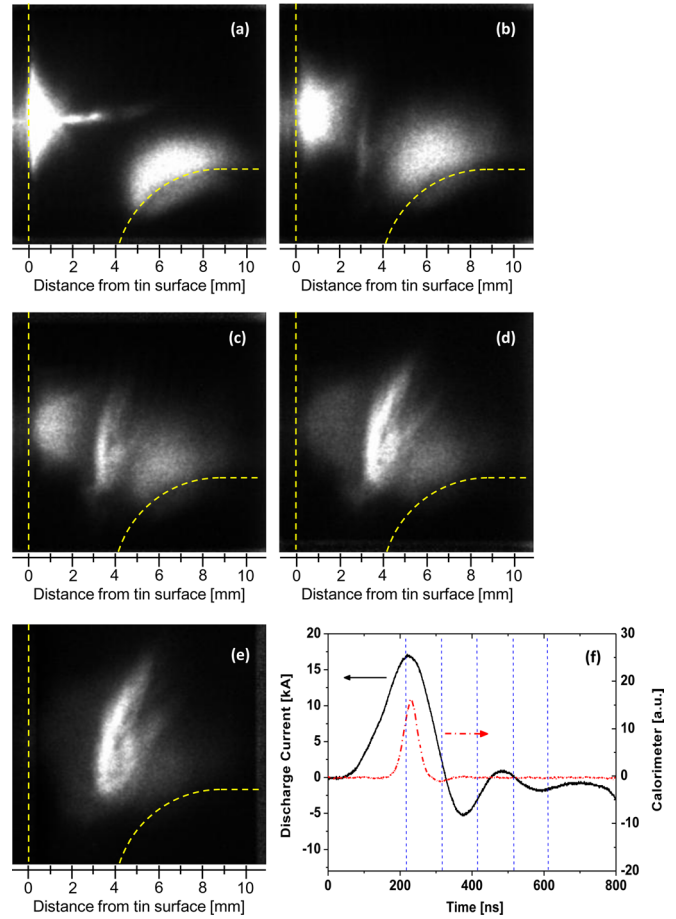


FIG. 7. (Color online) (a)-(e) Plasma behavior in the LDP EUV source captured by an ICCD camera with a 100 ns gate time. The dashed vertical lines and curves indicate the positions of the tin cathode and the anode, respectively. (f) Waveforms of discharge current (solid line) and in-band EUV emission (dashed-dotted line), with five dashed vertical lines that refer to the observation start times of (a)-(e).

with the plasma that attaches to the anode surface.²⁸ With the expansion of the anode and cathode plasmas, the plasma shell becomes even more obvious, with the visible-region emission lasting longer than that from the anode and cathode plasmas. Finally the plasma shell expands and decays with time.

In order to obtain specific temporal- and spatial-resolved parameters of the expansion plasmas in the decay phase in our LDP source, the above-mentioned intersection Stark broadening method is adopted in order to determine simultaneously the electron density n_e and temperature T_e using measured Sn II $5s^24f^2F^{\circ}_{5/2}-5s^25d^2D_{3/2}$ (558.9 nm) and $5s^26d^2D_{5/2}-5s^26p^2P^{\circ}_{3/2}$ (556.2 nm) spectral lines emitted from plasmas at 1 to 6 mm from the tin surface in the pinch axis. The spectra are recorded by a streak camera with a 200 ns gate time (400 ns for the position at 6 mm from the tin cathode). For each spatial and temporal condition, the spectrum is averaged over 4 discharges. An example of the plasma emission spectrum at 3 mm from the tin surface and 400 ns after the laser initiation is shown in Fig. 8. Besides the experimental data (black line with dots), the Voigt-fit curves of the individual lines are plotted by the blue dashed line and the red dashed-dotted line in this figure. With a measured instrumental broadening of 0.58 nm, the FWHM of

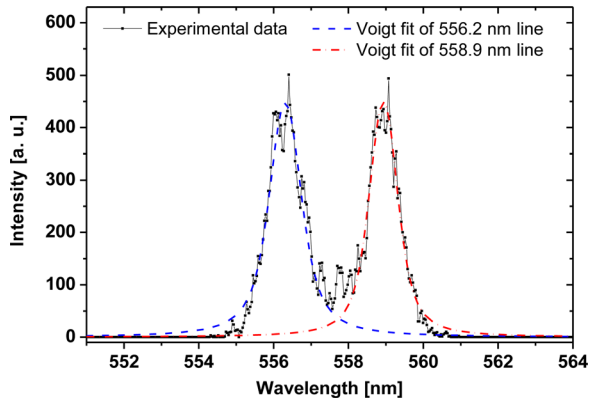


FIG. 8. (Color online) Example of the plasma spectrum of Sn II $5s^24f^2F^{\circ}_{5/2} - 5s^25d^2D_{3/2}$ (558.9 nm) and $5s^26d^2D_{5/2} - 5s^26p^2P^{\circ}_{3/2}$ (556.2 nm) lines at 3 mm from the tin surface, 400 ns after the laser initiation, recorded by the ICCD camera with a 200 ns gate time. In addition to the experimental data (solid line and dots), the Voigt-fit curves of individual lines are plotted (dashed line and dashed-dotted line).

the Stark broadening are obtained as 0.69366 ± 0.02133 and 0.53554 ± 0.01785 for Sn II 556.2 nm and 558.9 nm lines, respectively, from which n_e and T_e are obtained according to the intersection Stark broadening method (Figs. 2 and 1).

1. Electron temperature estimation

At each axial position observed, the Stark-width-ratio of the two Sn II lines is found to be almost constant with time, which indicates that the electron temperature T_e does not change much during the expansion process. This temperature freezing phenomenon was also noted in Ref. 29. At positions of 1 mm, 2 mm, and 6 mm from the cathode tin surface, $T_e \approx 0.40$ eV; at 3 mm, $T_e \approx 0.86$ eV; at 4 mm, $T_e \approx 1.0$ eV. According to the simulation results, T_e at the maximum implosion is 30 to 40 eV in a LDP source. Our results indicate that T_e drops to ~ 1 eV within 150 ns. The fast cooling observed after the maximum Z-pinch is due to adiabatic expansion, while the thermal energy converts to kinetic energy. Based on the theoretical model of the one dimensional adiabatic expansion of the collisionless plasma with a Gaussian spatial distribution of n_e , T_e evolution follows³⁰

$$T_e(t) = T_{e0} \frac{R_0^2}{R_0^2 + 2c_{s0}^2 t^2}. \quad (2)$$

Assume the following initial conditions at the maximum pinch: characteristic length $R_0 = 5$ mm, electron temperature $T_{e0} = 40$ eV, and charge state $Z_0 = 8$; the sound speed is calculated as $c_{s0} = 1.6 \times 10^4$ m s⁻¹. The T_e evolution will follow the curve in Fig. 9. This calculation result fits our experimental result very well (T_e drops to below 1 eV within 150 ns).

Moreover, given that the plasma expansion processes after the maximum Z-pinch and after the laser ablation are both dominated by adiabatic expansion into the vacuum, we compared our result with the electron temperature measured in a LPP EUV source using a bulk tin target.³¹ The Boltzmann plot measurement indicated that T_e at 1 mm from the target decayed to 1 eV within ~ 180 ns of the evolution of the laser ablation plume, and T_e at 2 mm remained around

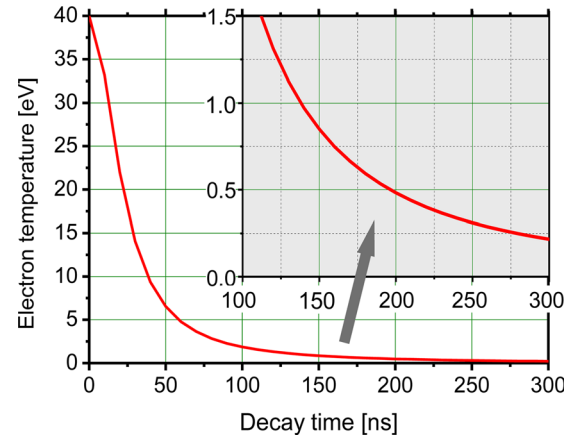


FIG. 9. (Color online) Electron temperature evolution [Eq. (2)] of the one-dimensional adiabatic expansion of the collisionless plasma with a Gaussian spatial distribution of n_e (Ref. 30). Assume the following initial conditions at the maximum pinch: characteristic length $R_0 = 5$ mm, electron temperature $T_{e0} = 40$ eV, and charge state $Z_0 = 8$.

1 eV during expansion. This experimental result and our T_e estimation also fit quite well. Good comparison with both the theoretical model and another group's measurements prove that the intersection Stark broadening method is a credible means of T_e estimation.

2. Electron density estimation

Electron density evolutions of the expansion plasma at different axial positions are plotted in Fig. 10. The time of each plotted point refers to the observation start time of the streak camera with respect to the laser incident moment. At the early stage of expansion, n_e at 3 mm has the largest value (3.56×10^{17} cm⁻³) compared with those at other positions. In addition, the decay curve of n_e at 3 mm displays a typical exponential decay tendency with time, with a decay time constant of 125 ns obtained from the first order exponential decay fitting. For positions nearer to the electrode, abnormal "increases" of n_e during the plasma decay are observed: 450 ns at 1 mm, 350 ns at 2 mm, 400 ns at 4 mm, and 550 ns at 6 mm. This phenomenon can be explained by the expansion of the plasma shell between the electrodes (Fig. 8(b)). The obvious plasma shell

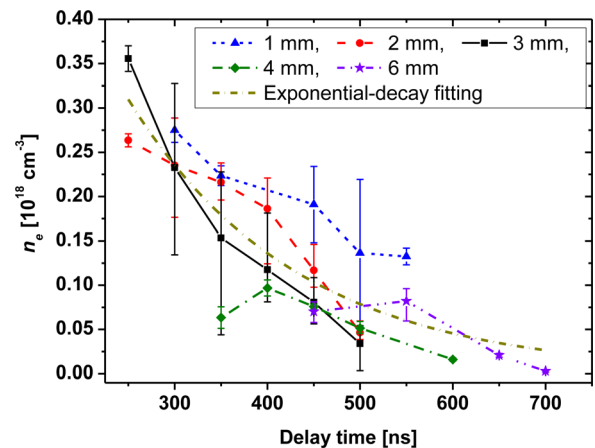


FIG. 10. (Color online) Electron density n_e evolution of the residue plasma in the LDP EUV source at different axial positions from the tin surface after a discharge; 0 ns refers to the laser initiation time.

indicates a sharp change of the plasma density. Therefore, due to its highest n_e (at 3 mm; 250 ns in Fig. 10), large n_e gradient, and particular position and shape, the plasma shell expands toward the cathode and anode, which causes local n_e “increases” at positions nearer to the electrodes. From the time and position of the local n_e “increases,” the expansion velocity of the center plasma shell is calculated as $\sim 1.2 \times 10^4 \text{ m s}^{-1}$ along the cathode axis toward both electrodes. These local n_e “increases” also indicate that the plasma expansion is the dominant reason for the n_e decay, other than the recombination process. This conclusion is also justified by the freezing process of the charge state distribution when arc plasmas expand into the vacuum.²⁹ By fitting the n_e values at all positions using the first order exponential decay function, as shown by the dark-yellow dashed line in Fig. 10, the n_e decay constant is estimated as $183 \pm 24 \text{ ns}$.

V. DISCUSSION

Because the plasma expansion processes after the maximum implosion in a LDP EUV source and after laser ablation in a LPP EUV source can both be considered as dominated by adiabatic expansion into the vacuum, and because the EUV-emitting plasmas in both sources have similar electron temperatures,^{8,9} we can safely assume that particles in these two cases share similar motion-patterns during expansion. In our previous study on the characteristics of LPP, the expansion behaviors of electrons and neutrals were investigated using Stark broadening and laser induced fluorescence, respectively. The density decay constant of electrons τ_e and neutrals τ_n were estimated as $\tau_e = 206 \text{ ns}$ and $\tau_n = 7.94 \text{ } \mu\text{s}$. Therefore, for the expansion plasma in our LDP source, τ_n is estimated to be $7.05 \text{ } \mu\text{s}$, proportional with $\tau_e = 183 \text{ ns}$ obtained in this experiment.

Because the expansion of the residual neutral gas directly affects the electrical recovery after a discharge, its decay constant determines the maximum repetition rate of EUV emissions in a LDP source. In order to guarantee that there will be no undesirable breakdown between two regular discharges for EUV generation, the mean free path of electrons λ_e needs to be at least 10 times the electrode gap distance; in our case, $\lambda_e \geq 100 \text{ mm}$. For weakly ionized plasmas, $\lambda_e = (\sigma_{e\text{-ionization}} \cdot n_n)^{-1}$, where $\sigma_{e\text{-ionization}}$ is the electron-impact ionization cross section and n_n is the neutral particle density. According to Refs. 32, 33, the maximum $\sigma_{e\text{-ionization}}$ for Sn atoms is $1 \times 10^{-15} \text{ cm}^2$. Thus, in order to achieve $\lambda_e \geq 100 \text{ mm}$, n_n needs to be less than $1 \times 10^{14} \text{ cm}^{-3}$.

For free expansion with a constant diffusion coefficient, the number density after a time span t can be expressed as $n_t = n_0 \exp(-t/\tau)$, where n_0 is the initial number density. For the LDP source, if we assume that each discharge produces atoms with a number density of N_0 and the discharge interval is T , the number density of the residue gas just before the $(i+1)$ th time of discharge (at the delay time of $i \cdot T$) is

$$N_f = N_0 \left[\left\{ \exp\left(-\frac{T}{\tau}\right) + 1 \right\} \exp\left(-\frac{T}{\tau}\right) + 1 \right] \exp\left(-\frac{T}{\tau}\right) \\ = N_0 \lim_{n \rightarrow \infty} \sum_{i=1}^n \exp\left(-i\frac{T}{\tau}\right) = N_0 \frac{\exp(-T/\tau)}{1 - \exp(-T/\tau)}. \quad (3)$$

For $T \gg \tau$, $N_f \approx N_0 \exp(-T/\tau)$. As the optimum atom density for EUV emission is $N_0 \leq 1 \times 10^{18} \text{ cm}^{-3}$ (Ref. 9) and the neutral density estimated for preventing undesirable discharge between electrodes is $N_f \leq 1 \times 10^{14} \text{ cm}^{-3}$, the interval T needs to be no less than 10 times the gas decay constant τ_n , $T_{\min} = 10\tau_n$, from Eq. (3). Therefore, in our case, $T_{\min} = 70.5 \text{ } \mu\text{s}$ with $\tau_n = 7.05 \text{ } \mu\text{s}$, and the maximum repetition rate is $\sim 14 \text{ kHz}$ accordingly. Considering that in the calculation we use the most secure values for each step of estimation, and that at the early stage of expansion after the maximum implosion ions and electrons that dominate the plasma composition expand with a much larger diffusion constant than that of the neutrals, the possible maximum discharge repetition rate could be larger than our estimated value.

VI. CONCLUSION

This article introduces an intersection method using Stark broadenings of two Sn II lines ($5s^2 4f^2 F^{\circ}_{5/2} - 5s^2 5d^2 D_{3/2}$ 558.9 nm and $5s^2 6d^2 D_{5/2} - 5s^2 6p^2 P^{\circ}_{3/2}$ 556.2 nm) to determine simultaneously the electron temperature T_e and density n_e of plasmas. In this method, the Stark-width-ratio of these two lines, which is independent of n_e , is used to estimate T_e based on the calculation results. Then n_e can be obtained according to the Stark width of each line. The validity of this diagnostic method is confirmed by the agreement between the calculation results of the He I $1s3d^1 D_2 - 1s2p^1 P^{\circ}_1$ line (667.8 nm) profiles and the experimental data obtained from tin fueled arc discharge in pure helium gas at atmospheric pressure.

This simple and inexpensive intersection Stark broadening method has been applied to obtain the spatial-resolved evolutions of T_e and n_e of the expansion plasma in the decay phase (50 to 900 ns after the maximum implosion) in our LDP EUV source. T_e is found to drop to below 1 eV within 150 ns after the maximum implosion. Different n_e decay characteristics along the Z-pinch axis imply that plasma expansion is the dominant cause for the n_e decrease. The expansion velocity of the electrons is estimated as $\sim 1.2 \times 10^4 \text{ m s}^{-1}$, from the plasma shell between electrodes towards the cathode and the anode. The decay time constant of n_e is $183 \pm 24 \text{ ns}$. Through comparison with the plasma expansion behavior in the LPP source, the decay constant of the residual neutral gas after a discharge is estimated as $7.05 \text{ } \mu\text{s}$.

Based on the theory of electron-impact ionization, the minimum time-span that electrical recovery between the electrodes needs in order to guarantee the next succeeding regular EUV-emitting discharge is estimated to be $70.5 \text{ } \mu\text{s}$, which indicates that the maximum repetition rate is $\sim 14 \text{ kHz}$. Given that the in-band EUV energy of our LDP source working in the single-pulse-mode was estimated as $8.9 \text{ mJ}/(2\pi\text{sr})$, the output can reach $125 \text{ W}/(2\pi\text{sr})$, if it works at the maximum repetition rate. This estimation indicates that our LDP source has the potential to be utilized for EUV metrology.

Before we can discuss possible ways to increase the repetition rate, further experimental and theoretical efforts are necessary in order to obtain more specific temporal- and

spatial-resolved neutral density distributions between the electrodes, and to clarify the diffusion behaviors and their contributions toward the electrical recovery process after a discharge.

ACKNOWLEDGMENTS

Q. Zhu is very grateful to Dr. Tohru Kawamura of Department of Energy Sciences in Tokyo Institute of Technology for his patience and really helpful discussions. Many thanks also to Nac Image Technology Inc. for the ICCD camera ULTRA Neo and the technical support they offered.

¹B. Wu and A. Kumar, *Extreme Ultraviolet Lithography* (McGraw-Hill, New York, 2009).

²V. Bakshi, *EUV Source for Lithography* (SPIE, Bellingham, WA, 2006).

³G. Vandentop, in Proceedings of the 7th Annual SEMATECH Symposium and ISMI Regional Meeting Series in Japan, Tokyo, Japan, 22 June, 2011.

⁴H. Meiling, V. Banine, P. Kuerz, and N. Hamed, *Proc. SPIE* **5374**, 31 (2004).

⁵J. Pankert, R. Apetz, M. Janssen, J. Jonkers, A. List, M. Loeken, G. Simons, D. Vaudrevange, D. Wagemann, O. Zitzen, K. Bergmann, J. Klein, W. Neff, S. Probst, R. Prummer, O. Rosier, S. Seiwert, G. Derra, T. Kruecken, C. Metzmacher, A. Weber, and P. Zink, *Proc. SPIE* **5751**, 260 (2005).

⁶Y. Teramoto, T. Yokoyama, H. Mizokoshi, H. Sato, and K. Hotta, *Proc. SPIE* **7271**, 727139 (2009).

⁷M. Yoshioka, Y. Teramoto, P. Zink, G. Schriever, G. Niimi, and M. Corthout, *Proc. SPIE* **7636**, 763610 (2010).

⁸M. Masnavi, M. Nakajima, E. Hotta, K. Horioka, G. Niimi, and A. Sasaki, *J. Appl. Phys.* **101**, 033306 (2007).

⁹A. Sasaki, K. Nishihara, A. Sunahara, H. Furukawa, T. Nishikawa, and F. Koike, *Proc. SPIE* **7271**, 727130 (2009).

¹⁰Q. Zhu, J. Yamada, N. Kishi, M. Watanabe, A. Okino, K. Horioka, and E. Hotta, *J. Phys. D: Appl. Phys.* **44**, 145203 (2011).

¹¹H. Griem, *Spectral Line Broadening by Plasmas* (Academic, London, 1974).

¹²H. Griem, *Principles of Plasma Spectroscopy* (Cambridge University Press, Cambridge, England, 1997).

¹³J. Torres, J. Jonkers, M. J. van de Sande, J. J. A. M. van der Mullen, A. Gamero, and A. Sola, *J. Phys. D: Appl. Phys.* **36**, L55 (2003).

¹⁴H. R. Griem, *Phys. Rev.* **165**, 258 (1968).

¹⁵M. Seaton, *Atomic and Molecular Processes* (Academic, New York, 1962).

¹⁶H. van Regemorter, *Astrophys. J.* **136**, 906 (1962).

¹⁷W. McCormick and R. Sawyer, *Phys. Rev.* **54**, 71 (1938).

¹⁸C. Colón, and A. Alonso-Medina, *Astron. Astrophys.* **422**, 1109 (2004).

¹⁹U. Safronova, M. Safronova, and M. Kozlov, *Phys. Rev. A* **76**, 022501 (2007).

²⁰A. Alonso-Medina and C. Colon, *Phys. Scr.* **61**, 646 (2000).

²¹A. Alonso-Medina, C. Colon, and C. Rivero, *Phys. Scr.* **71**, 154 (2005).

²²P. Oliver and A. Hibbert, *J. Phys. B* **43**, 074013 (2010).

²³M. Miller, R. Roig, and R. Bengtson, *Phys. Rev. A* **20**, 499 (1979).

²⁴B. Martinez and F. Blanco, *J. Phys. B* **32**, 241 (1999).

²⁵H. Griem, M. Baranger, A. Kolb, and G. Oertel, *Phys. Rev.* **125**, 177 (1962).

²⁶W. Wiese and J. Fuhr, *J. Phys. Chem. Ref. Data* **38**, 565 (2009).

²⁷B. Omar, *Journal of Atomic, Molecular, and Optical Physics* **2011**, 850807 (2011).

²⁸Q. Zhu, J. Yamada, N. Kishi, M. Watanabe, A. Okino, K. Horioka, and E. Hotta, "Pinch dynamics of the 13.5 nm EUV-emitting plasma in a LA-DPP source" Proc. IEEE (submitted).

²⁹A. Anders, *Phys. Rev. E* **55**, 969 (1997).

³⁰P. More, *Phys. Plasmas* **12**, 112102 (2005).

³¹S. S. Harilal, Beau O'Shay, and M. S. Tillack, *J. Appl. Phys.* **98**, 013306 (2005).

³²M. Talukder, S. Bose, M. Patoary, A. Haque, M. Uddin, A. Basak, and M. Kando, *Eur. Phys. J. D* **46**, 281 (2008).

³³P. Bartlett and A. Stelbovics, *At. Data Nucl. Data Tables* **86**, 235 (2004).